ARTICLE IN PRESS
Ad Hoc Networks xxx (2015) xxx–xxx
Contents lists available at ScienceDirect
Ad Hoc Networks
journal homepage: www.elsevier.com/locate/adhoc

Underwater electromagnetic communications using conduction – Channel characterization

Arsen Zoksimovski [a,*], Daniel Sexton [b], Milica Stojanovic [a], Carey Rappaport [a]

[a] Northeastern University, Boston, MA, United States
[b] GE Global Research, Niskayuna, NY, United States

ARTICLE INFO

Article history:
Received 9 February 2014
Received in revised form 11 July 2014
Accepted 28 January 2015
Available online xxxx

Keywords:
RF conduction
Channel modeling
Capacity

ABSTRACT

Wireless underwater transmission is considered using electric field generated by a pair of electrodes with opposite current and detected by two receiving electrodes. Experiments were conducted at frequencies between 100 kHz and 6.35 MHz, using orthogonal frequency division multiplexing (OFDM). Our lab tests were performed in a plastic tank filled with salt water, and our sea test at the ocean surface and at 5 m depth (boundary free). Magnitude and phase-delay of the channel transfer function were modeled based on inference from dipole radiation theory in conducting medium. An exponential attenuation model fitted to the lab measurements indicated inverse cubic range dependence (near-field compliant). A rational-polynomial model provided the best match for the recorded magnitude, especially at low frequencies. Based on the exponential attenuation model, we estimated that the capacity of this channel is on the order of 10 Mbps in the 100 kHz–6.35 MHz band when inside half a meter radius with 1 W of transmit power, suitable for contactless data collection by remotely operated vehicles from single or multiple nodes via spectrum sharing. Finally, estimation of the effect range uncertainty of ±0.5 m can have on the achievable data rates showed up to 30% performance downtrend for 1 m range.

1. Introduction

Applications of electromagnetic field in underwater communications are short range transmission (<100 m) and very short range (<1 m), very high speed, transmission. Although our research is mostly concerned with propagation channel modeling [1], this technology supports the vision of a subsea positioning system – a network of devices scattered across the seabed that is used to guide ROVs to data collection sites mounted on production assets. When the vehicle is within close proximity of a data collection port, as illustrated in Fig. 1, it can transfer information at tens or hundreds of Mbps.

Two technically feasible RF conduction based designs for voice communication underwater were reported in [2]; one for divers (150 m range with 6 W of power), and the other for manned submersibles (1 km range with 280 W of power). Center frequency reported in the paper was 1.2 kHz, with bandwidth 1.5 kHz.

In [3], based on sea water frequency response obtained by transmitting a 1 μs pulse, it was shown that RF conduction method can deliver information at 1 Mbps for binary system. Another article has been published recently about a high-speed underwater RF solution using conduction [4], where the highest data rate reported was 1 Mbps at ranges 0.5 m, 0.8 m and 1 m.

Kelley et al. [5] described an orthogonal frequency division multiplexing (OFDM) solution for underwater RF communication. They performed simulations using BPSK, QPSK and QAM16, using frequencies between 0 MHz and

* Corresponding author.
E-mail address: zoksimovski.a@husky.neu.edu (A. Zoksimovski).

http://dx.doi.org/10.1016/j.adhoc.2015.01.017
1570-8705/

10 MHz. In addition, they simulated Alamouti space–time diversity and channel coding using rate 1/3 turbo codes. They assumed Ricean fading if there were line-of-sight component, while the path-loss models followed the work from [6]. The authors of [5] estimated through simulation that with 1 W of transmit power, a 1.14 Mbps RF data rate could be possible out to 60 m and 400 kbps out to 1 km in 10 MHz bandwidth.

Properties of underwater RF communication channel are discussed in a number publications related to underwater wireless sensor networks, such as [7,8]. Section 2 gives background on electromagnetic field in conducting media based on the electric dipole antenna model.

In Section 3 we describe the system components and the experiment. Like Kelley et al. [5], we chose OFDM as the transmission method. An advantage of OFDM over single-carrier schemes is its ability to cope with frequency-dependent channel attenuation without complex equalization filters. In this respect, underwater RF channel is similar to a copper wire channel because of its time-invariance and frequency-dependent attenuation profile.

Section 4 presents the channel frequency response models for magnitude and phase, derived from the experimental data based on the theory of electric dipole in a conducting medium. Using those models, in Section 5 we present a capacity analysis for this channel, and discuss the impact of range mismatch on the achievable rate. With an ad hoc sensor network in mind, this analysis is expected to provide insight into node spacing limitations. Depending on the bit rate constraints, we envision spectrum sharing between multiple nodes. For example, there could be an OFDM downlink, for functions such as handshaking, subcarrier assignment and channel sounding, while uplink could be multiple-access OFDM (OFDMA) where each transmit node would utilize a portion of available subcarriers assigned by the master node. Section 6 concludes the paper.

2. Propagation model

It is a well known concept that an RF conduction antenna can be analyzed as electric dipole in conducting medium if a solution to the Helmholtz equation is found by factoring conductivity in the complex-valued propagation constant that we will see below. The effects of underwater propagation and ohmic losses due to relatively high conductivity of seawater are taken into consideration by factoring the conductivity into the frequency dependent propagation constant. Here we focus on the segments of the theory of electric dipole in a conducting medium that are most relevant to our channel model formulation.

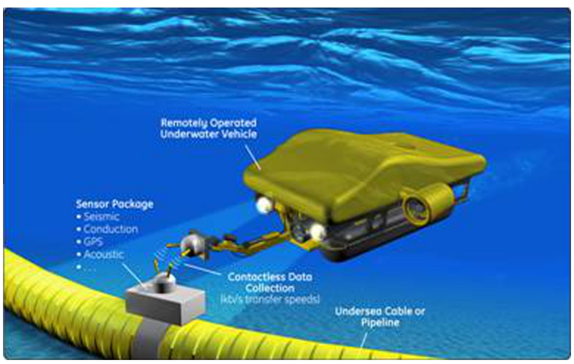

Fig. 1. ROV data upload.

There are three electromagnetic field components of a linear dipole antenna: radial and tangential electric fields E_r and E_θ, and magnetic field H_ϕ. The geometry of the antenna leads to coupling primarily of the E_θ component (the dipoles are parallel with centers in the same plane). It can be shown [9] that the tangential component of the electric field radiated by the infinitesimal dipole, at radial distance r from the source, is given by

$$E_\theta = j\eta \frac{kI_0 l \sin\theta}{4\pi r}\left(1 + \frac{1}{jkr} - \frac{1}{(kr)^2}\right)e^{-jkr} \qquad (1)$$

where l is the antenna length and I_0 the current. The complex-values propagation constant k is a function of radial frequency ω, given by

$$k = \beta - j\alpha = \omega\sqrt{\mu\varepsilon\left(1 - j\frac{\sigma}{\omega\varepsilon}\right)} \qquad (2)$$

where μ, ε, and σ are the permeability, permittivity and conductivity of the propagation medium, respectively. The characteristic impedance η of the medium is given by

$$\eta = \sqrt{\frac{\mu}{\varepsilon}\left(1 - j\frac{\sigma}{\omega\varepsilon}\right)^{-1}} \qquad (3)$$

The electric field (1) can be expressed as

$$E_\theta = E(\omega, r)e^{-\alpha r}e^{-j(\beta r + \vartheta(\omega, r))}$$

For a given range $r, E(\omega, r)$ has rational polynomial form in terms of ω. The product βr represents the propagation delay of the electromagnetic wave, while $\beta r + \vartheta(\omega, r)$ is the phase of the electric field.

Frequency variation of the magnitude of tangential electric field component between 0 Hz and 6.5 MHz is

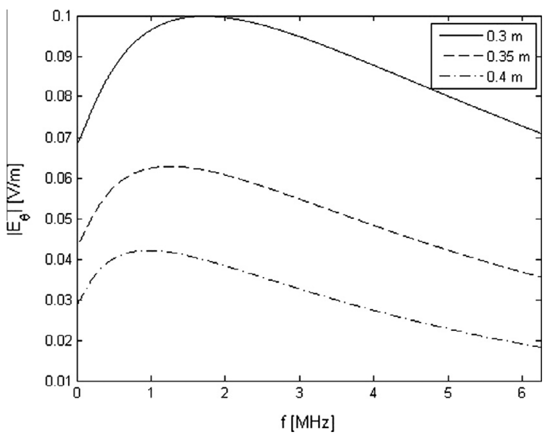

Fig. 2. Tangential electric field component magnitude as a function of frequency for several transmitter–receiver distances. $I_0 = 1$ A. Dipole length $l = 10$ cm.

illustrated in Fig. 2. We can see that the peak frequency decreases as range increases, eventually approaching zero. That trend is consistent with the notion of attenuating plane waves, whose far-field approximation in terms of frequency f is

$$E(r,f) \sim E_o exp\left(-a_o r\sqrt{f}\right) \quad (4)$$

for some $a_0 > 0$.

At frequencies such that $\sigma \gg 2\pi f\varepsilon$,

$$\alpha = \beta \simeq \sqrt{\pi f \mu_0 \sigma} \quad (5)$$

By substituting Eqs. (2) and (3) in (1) it can be shown that the phase of the tangential electric field, shown in Fig. 3, has a closed form expression given by

$$\vartheta(\omega) = tan^{-1}\left[\frac{\omega\mu\sigma r^2 + \beta r}{\omega^2\mu\varepsilon r^2 - 1 - \alpha r}\right] - \frac{1}{2}\cot^{-1}\left[\frac{\omega\varepsilon}{\sigma}\right] + \frac{\pi}{2} \quad (6)$$

Finally, the wavelength is defined as

$$\lambda = \frac{2\pi}{\beta} \quad (7)$$

With the approximation (5), $\lambda \approx \sqrt{\frac{4\pi}{f\mu\sigma}}$. Since $\mu \approx \mu_0 \approx 4\pi \times 10^{-7}\,\frac{H}{m}$,

$$\lambda \approx \sqrt{\frac{10}{f_{\mathrm{MHz}} \cdot \sigma}} \quad (8)$$

where f_{MHz} denotes frequency in MHz.

3. System overview

In order to measure the frequency response of an RF conduction channel, we transmitted and received data at multiple frequencies using RF conduction antennas. For our channel frequency response measurements, we used OFDM signals with $K = 128$ carriers, total bandwidth $B = 6.25$ MHz, lower band edge $f_0 = 100$ kHz, sub-carrier spacing $\Delta f = 48.83$ kHz. There were BPSK and QPSK modulated OFDM symbols in our streaming sequences, where the BPSK symbols were used for channel frequency response measurements. With QPSK modulated carriers, the bit rate used in the experiments was $R = 2 \cdot B = 12.5$ Mbps. Note that a practical system would reserve some carriers for pilots and employ additional channel coding, which would reduce the effective bit rate.

The waveforms were designed in Matlab and hard-coded into the transmitter's FPGA module. Following the acquisition through the data capture board in the receiving unit, the received signals were post-processed in Matlab to obtain the channel frequency response.

Our lab tests were conducted in a plastic tank filled with salt water. The results shown in Section 4 correspond to the distance between the transmitter and the receiver of 35 cm and 50 cm, shown in Fig. 4.

The experiment in the ocean was carried out at a depth of approximately 5 m. (Skin depth at 100 kHz is approximately 0.77 m.) We also performed a set of measurements very close to the surface. Conductivity of the water was measured to be 1.3 S/m in the tank and 4.3 S/m in the ocean. For the sea test, the transmitter and receiver containers were mounted on a steel frame, as shown in Fig. 5. The separation distance between the tips of the electrodes of the transmitter and the receiver was about 10 cm. The entire frame was lowered into the water from a small boat to collect data.

Transmitter was a completely self-contained unit, battery-powered with no connection to the outside world. A waveform generator, controlled by the FPGA, was used to form the signals. After D/A conversion, the signals were smoothed using a filter and presented to the output driver. The output driver produces 1A current to supply the electrodes. The dynamic range of the D/A converter was 2 V peak-to-peak. The electronics and batteries sufficient to drive the transmitter over several hours (10 NiMH batteries) were placed inside a 4-in. PVC pipe container which was sealed to make it pressure-resistant to 5 m depths. The electrodes were small pieces of $\frac{1}{4}$-in. copper pipe. The separation between electrodes was determined by the mechanical constraints of the package, and the length of

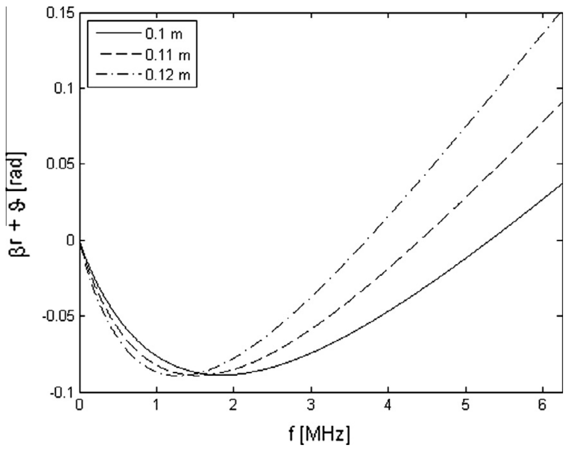

Fig. 3. Tangential electric field component phase as a function of frequency for several transmitter–receiver distances. $I_0 = 1$ A. Dipole length $l = 10$ cm.

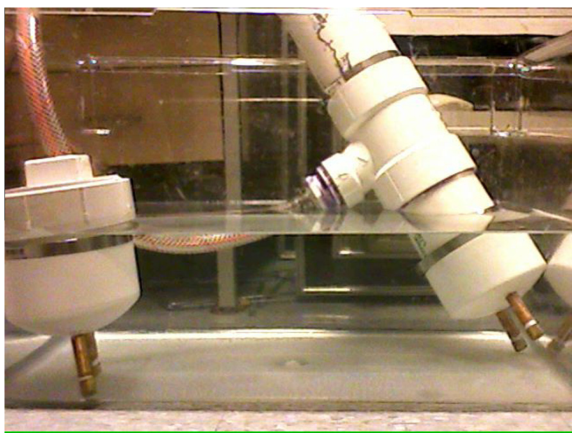

Fig. 4. Lab tank.

Please cite this article in press as: A. Zoksimovski et al., Underwater electromagnetic communications using conduction – Channel characterization, Ad Hoc Netw. (2015), http://dx.doi.org/10.1016/j.adhoc.2015.01.017

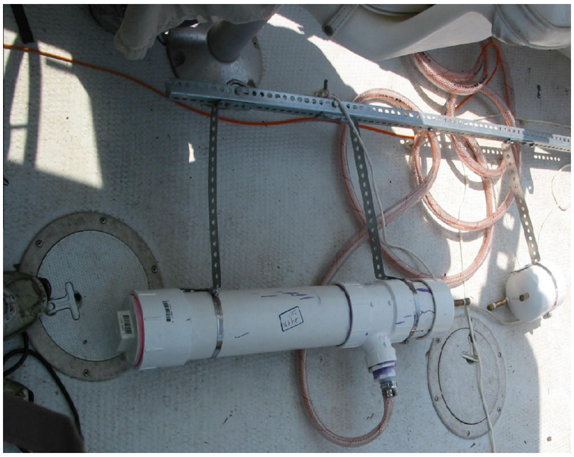

Fig. 5. The frame holding the transmitter (smaller tube) and the receiver.

the electrodes was set so as not to exceed the current drive of the transmitter. The transmitter is capable of producing waveforms up to 10 MHz. A Spartan FPGA was used as the arbitrary waveform generator with clock frequency of 51.6096 MHz.

The receiver utilized a data capture 14 bit acquisition card from Linear Technologies and a Fiber Optic USB connection so that no copper connection was made to the receiver. External 50 MHz clock source was designed and implemented by GE Research. The electronics were battery-powered and capable of several hours of operation. A pre-amplifier, model ZFL-1000LN+ (15 V) by Mini-Circuits, was included to keep the input signal within range of the A/D converter (1.5 V peak-to-peak).

4. Channel frequency response

Since our experimental signals represent voltage between the receiving electrodes, we expect that the measured channel frequency response should match the electric field function discussed in Section 2. We investigate this match by fitting the measured data to parametric models devised from (1) and (4).

Not counting the noise, the transmitted and the received signal are related by

$$Y(r_0,f) = H(r_0,f)X(f)$$

where $H(r_0,f)$ is the channel transfer function corresponding to a range r_0. For shorter notation, we write $H(f) = H(r_0,f)$, or sometimes just H. Our goal here is to model the magnitude and the phase of the function

$$H(f) = |H(f)|e^{j\varphi(f)}$$

4.1. Magnitude of the channel frequency response

The simplest propagation model known in theory is the exponentially attenuating wave approximation. Referring to (4), we assume

$$|H| = A_0 e^{-\alpha_1\sqrt{f}} \tag{9}$$

where A_0 and α_1 represent the model parameters. The relation between (4) and (9) suggests that $\alpha_1 \sim \alpha_0 r$. This approximation is notably valid when the receiver is in the far-field. It can be seen from (8) that if the frequency is not higher than 10 MHz and $\sigma \approx 4$ S/m, the wavelength is not shorter than half a meter. The far-field boundaries at 100 kHz and 6.35 MHz, respectively, are $5\,\text{m}/2\pi \approx 80$ cm and $0.6\,\text{m}/2\pi \approx 10$ cm. Since our measurements correspond to ranges on the order of 10–50 cm, we can see that the receiving antenna was in a combination of near- and far-fields.

If the propagation medium is not treated strictly as highly conducting, (2) suggests that we can assume linear frequency dependence of the exponential attenuation constant. Another simple model is then given by

$$|H| = A_0 e^{-\alpha_2 f} \tag{10}$$

where A_0 and α_2 are the representing parameters. A more general model can be formulated as

$$|H| = \frac{p_1 f^2 + p_2 f + p_3}{q_1 f^2 + q_2 f + q_3} \cdot e^{-\alpha_3 f} \tag{11}$$

The rational-polynomial part of this model was derived by substituting (2) into (1) and finding the magnitude. This model is better suited to near-field situations than (9) and (10) in the sense that it allows for magnitude dependence on frequency. It is described by a set of seven parameters: $p_1, p_2, p_3, q_1, q_2, q_3, \alpha_3$.

4.2. Phase model

Referring to the expression (6), when $\omega\varepsilon \ll \sigma$, as it is the case in well conducting medium such as sea water, we have that

$$cot^{-1}\left[\frac{\omega\varepsilon}{\sigma}\right] \approx \frac{\pi}{2} - \frac{\omega\varepsilon}{\sigma} \approx \frac{\pi}{2}$$

The combined effect of the βr component and the tan^{-1} component can be captured by a combination of linear and square-root frequency terms. Incorporating these approximations into the expression (6) leads to a relatively simple model for the channel phase:

$$\varphi(f) = -b\sqrt{f} + cf + d \tag{12}$$

where b, c, and d represent fitting parameters of the model.

4.3. Data Fitting

We used the measurements from the lab and the field to fit our models, based on non-linear function least-square fitting. Fig. 6 shows the measured channel characteristics along with the models (9)–(11) for the magnitude and (12) for the phase. The corresponding measurements are taken in the tank, at 35 cm range. The channel magnitude varies between −54 dB and −34 dB in the given frequency band.

Fig. 7 shows the channel characteristics measured in the tank at 50 cm range. Again, the magnitude is described by the expressions (9)–(11) and the phase by (12). Channel magnitude at 50 cm distance varies between −60 dB and

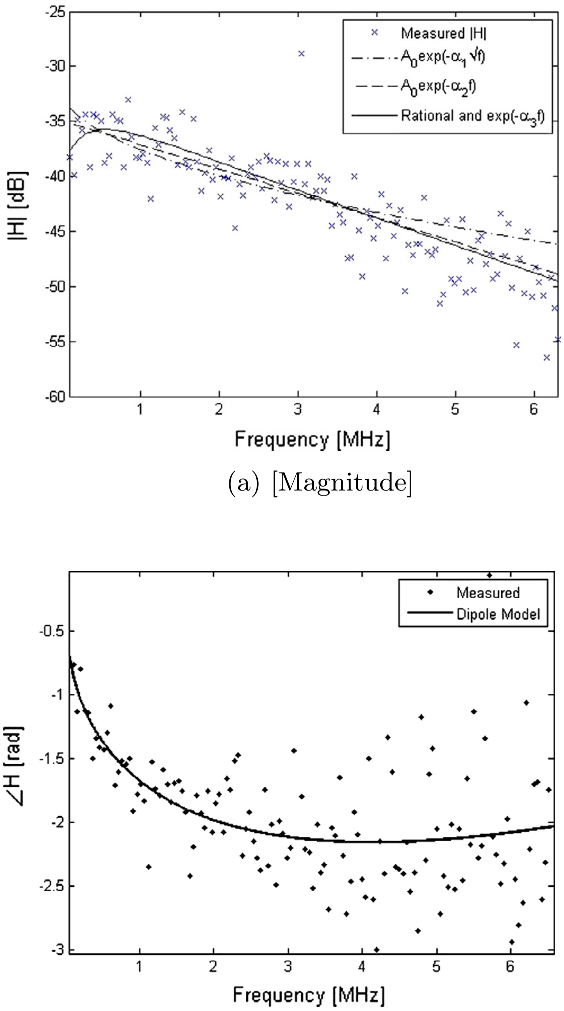

(a) [Magnitude]

(b) [Phase]

Fig. 6. Channel magnitude and phase: measured values in the tank and models (9)–(11) for the magnitude and (12) for the phase. Range 35 cm.

−45 dB in the given frequency band. Compared to the 35 cm range results, that indicates approximately 6 dB attenuation at the high end of the frequency band and 11 dB at the low end.

We notice that the phase at the longer range is folded upward more so than at the shorter range (Fig. 6). This tendency can be predicted based on the theory, as illustrated in Fig. 3; however, theoretical prediction of the minimum frequency for the given separation distance is significantly lower than the measurement. Therefore, space-constrained environment and the vicinity of the boundaries in the tank may dictate a different phase model than the one given by (1) and (6), which corresponds to a boundary-free environment.

Fig. 8 shows the channel characteristics measured at the ocean surface, and Fig. 9 corresponds to 5 m depth. The magnitude is again characterized by (9)–(11) and the phase by (12).

Based on the results shown in Figs. 8 and 9, the channel frequency response close to the surface shows a much lower attenuation, probably because part of the electromagnetic energy was reflected from the ocean-air boundary. In the given frequency band, the channel magnitude varies between −75 dB and −55 dB at the surface, and between −100 dB and −75 dB at 5 m depth. Therefore, the proximity of the ocean surface, as a reflecting boundary, results in 25 dB and 20 dB stronger signal at the high and low ends of the frequency band, respectively.

As expected, the rational-polynomial model (11) provides the best match for the recorded magnitude characteristic. This is notably true at low frequencies where the far-field assumption does not hold, and both models (9) and (10) fail to capture the effect. Beyond the peak frequency, model (10) gives a better match than model (9), but is still outperformed by the rational-polynomial model (11).

As for the phase, it is interesting to observe a broad minimum at around 2 MHz in Figs. 8 and 9. According to

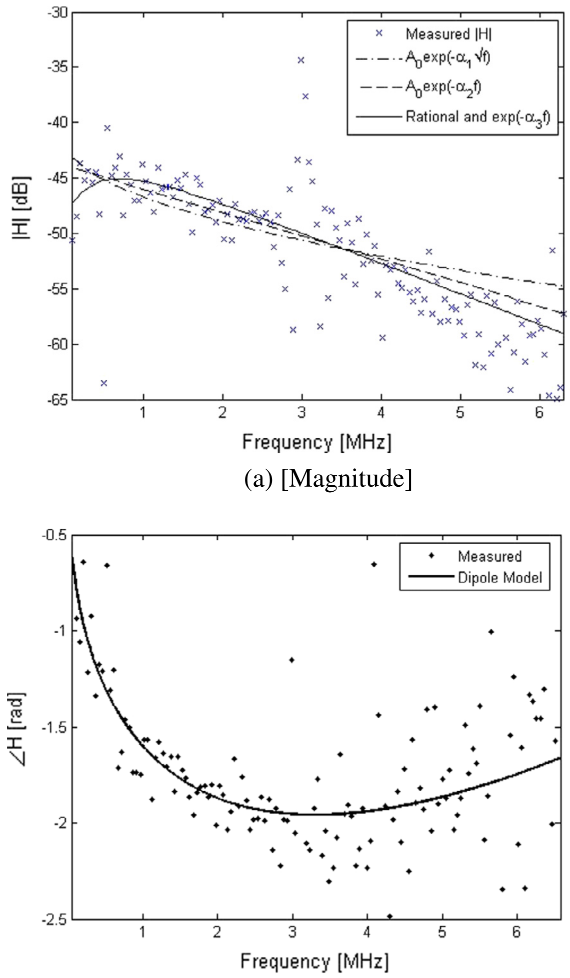

(a) [Magnitude]

(b) [Phase]

Fig. 7. Channel magnitude and phase: measured values in the tank and models (9)–(11) for the magnitude and (12) for the phase. Range 50 cm.

Please cite this article in press as: A. Zoksimovski et al., Underwater electromagnetic communications using conduction – Channel characterization, Ad Hoc Netw. (2015), http://dx.doi.org/10.1016/j.adhoc.2015.01.017

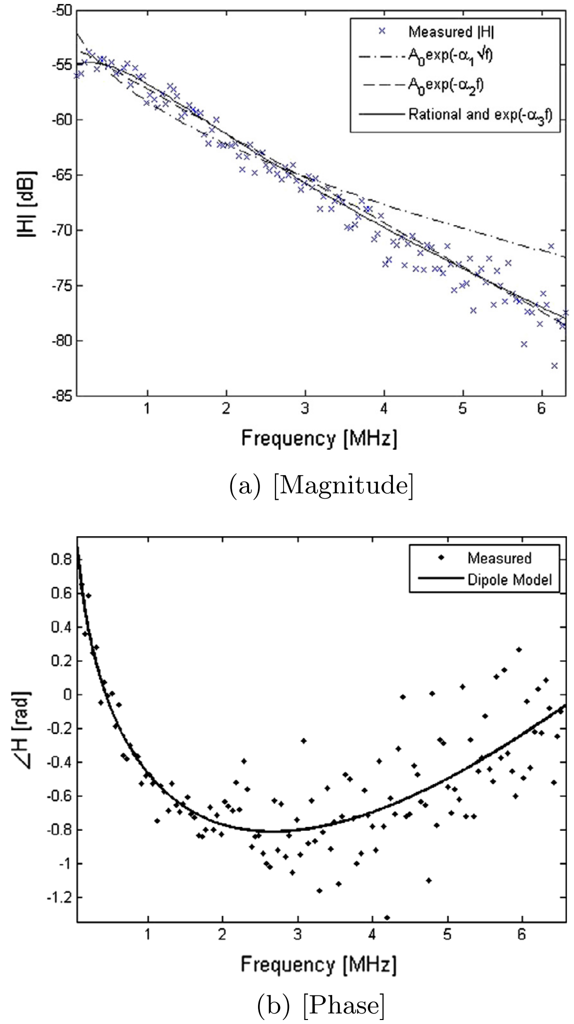

Fig. 8. Channel magnitude and phase: measured values at sea surface, and models (9)–(11) for the magnitude and (12) for the phase. Range 10 cm.

the theory of electric dipole, that would indicate a separation distance of around 10 cm, which coincides with the distances between the tips of the transmit and receive electrodes in the experiment.

In Figs. 6–9, the sea test data appear less scattered than the tank test data. In particular, sea test data at 5 m depth appear even less scattered than the sea test data from the surface measurements, which can be justified by the fact that there is less noise at 5 m depth than at the surface.

Tables 1–4 list the model parameters corresponding to the expressions (9)–(11), with frequency in MHz. Each table contains entries for two lab tests and two sea tests. Results that correspond to the measurements in the tank at 35 cm and 50 cm range are referred to as Lab 1 and Lab 2, respectively. Tests Sea 1 and Sea 2 correspond to the measurements at the sea surface and 5 m deep, respectively.

The A_0 values shown in Tables 1 and 2 indicate r^{-3} dependence. That is in agreement with (1) for $kr \ll 1$, or near-field.

Table 1
Channel transfer function magnitude fitting parameter values. Model given by (9).

$A_0 exp\left(-\alpha_1 \sqrt{f}\right)$	A_0	α_1
Lab 1	2.55e−2	0.6562
Lab 2	8.56e−3	0.617
Sea 1	3.54e−3	1.073
Sea 2	3.35e−4	1.011

Table 2
Channel transfer function magnitude fitting parameter values. Model given by (10).

$A_0 exp(-\alpha_2 f)$	A_0	α_2
Lab 1	1.8e−2	0.2551
Lab 2	6.4e−3	0.2437
Sea 1	2.2e−3	0.4652
Sea 2	2.1e−4	0.4129

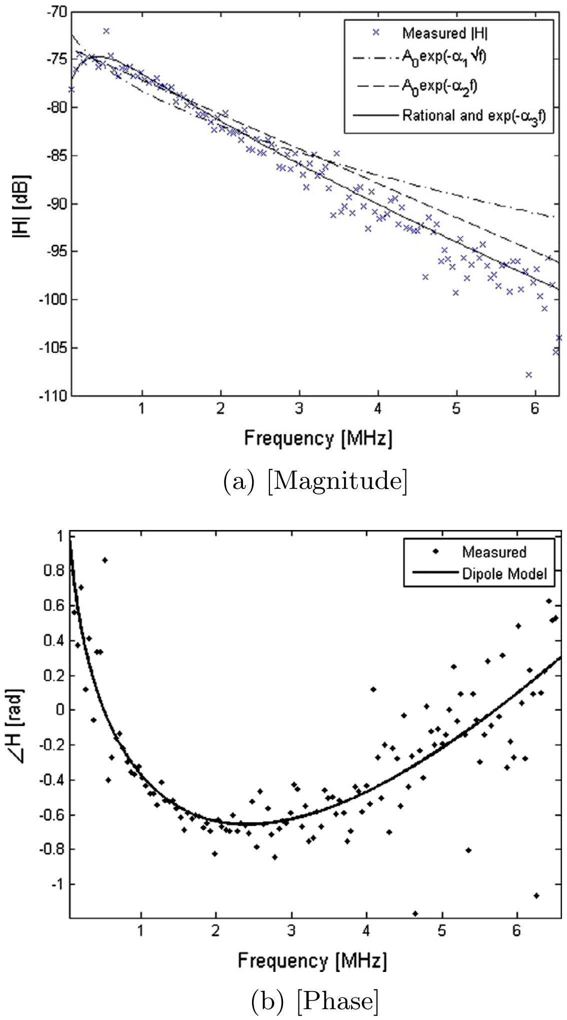

Fig. 9. Channel magnitude and phase: measured values at sea, at 5 m depth, and models (9)–(11) for the magnitude and (12) for the phase. Range 10 cm.

Please cite this article in press as: A. Zoksimovski et al., Underwater electromagnetic communications using conduction – Channel characterization, Ad Hoc Netw. (2015), http://dx.doi.org/10.1016/j.adhoc.2015.01.017

Table 3
Channel transfer function magnitude fitting parameter values for dipole model given by (11).

	p_1	p_2	p_3	q_1	q_2	q_3	α_3
Lab 1	0.0110	0.0104	0.0024	0.5993	0.3488	0.2271	0.2776
Lab 2	0.0066	0.0043	0.0014	0.7913	0.4794	0.3735	0.3196
Sea 1	−1.944e−5	3.467e−4	3.32e−4	0.1082	0.0857	0.1913	0.1615
Sea 2	3.426e−5	1.15e−4	1.48e−5	0.3655	0.2179	0.1627	0.3894

Table 4
Channel transfer function phase fitting parameter values. Model given by (12).

$\varphi(f)$	b	c	d
Lab 1	1.817	0.4464	−0.3061
Lab 2	1.936	0.5326	−0.1996
Sea 1	2.803	0.8589	1.477
Sea 2	2.898	0.9342	1.591

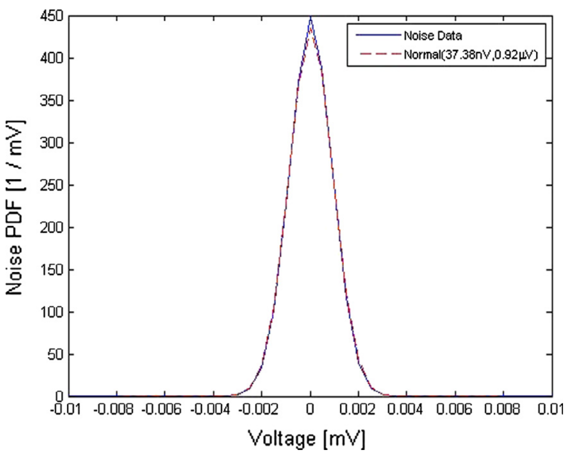

(a) [Without antenna]

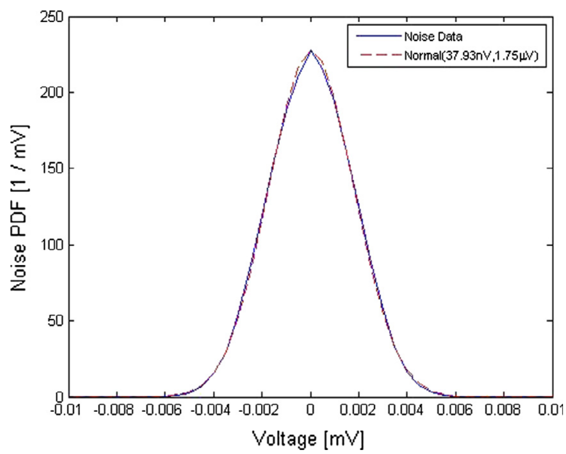

(b) [With antenna]

Fig. 10. Noise PDF measured in the lab.

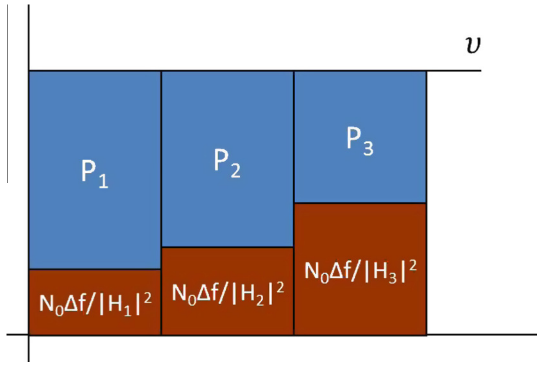

Fig. 11. Water-filling solution: the power allocated to each subcarrier is shown in light color. (For interpretation of the references to colour in this figure legend, the reader is referred to the web version of this article.)

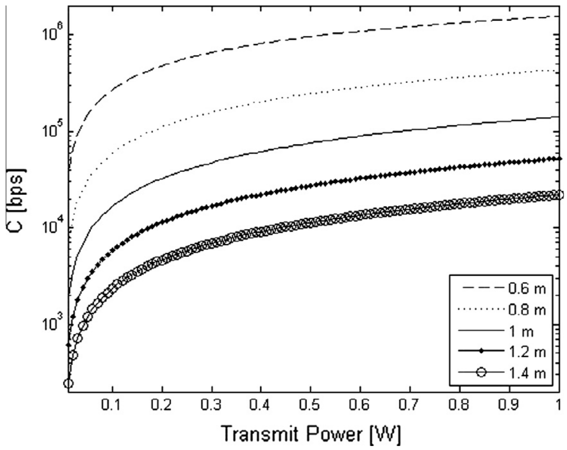

Fig. 12. Capacity vs. power for several different ranges and the 100 kHz–6.35 MHz band. Channel frequency response model (10) of Sea 2 (5 m depth) is used.

5. Capacity estimation

Based on the channel models derived in previous sections, we estimate the capacity of the underwater RF channel using the well known Shannon–Hartley formula for additive white gaussian noise (AWGN) channels. We measured the probability distribution function (PDF) of the noise, shown in Fig. 10, which closely matches Gaussian distribution. With no antenna connected to the receiver's A/D converter, this noise represents the actual receiver

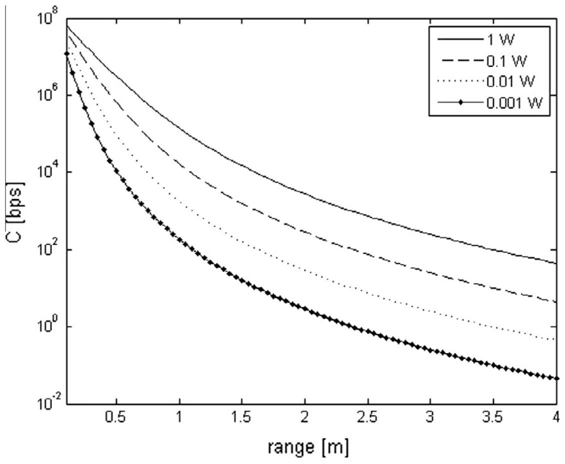

Fig. 13. Capacity vs. range for four different transmit power values and the 100 kHz–6.35 MHz band. Channel frequency response model (10) of Sea 2 (5 m depth) is used.

noise as the antenna itself is part of the channel. Adding the RF conduction antenna to the receiver increased the noise variance, while the PDF remained Gaussian. Based on our measurements in the ocean, we estimated a reasonably flat power spectral density (PSD) of the noise at -165 ± 1 dBm/Hz.

The capacity of parallel band-limited AWGN channels is given by [10]

$$C = \sum_{k=1}^{K} \triangle f \cdot log_2\left(1 + \frac{P_k |H_k|^2}{N_0 \triangle f}\right) \tag{13}$$

where P_k denotes the power transmitted on the k-th AWGN channel (k-th subcarrier of an OFDM system) and $\triangle f$ represents the subband width. N_0 is the PSD of the noise, i.e. the product $N_0 \triangle f$ can be interpreted as the power of the noise contained within the frequency band of the k-th subchannel. The optimal power allocation for which the capacity (13) is maximized is given by the well-known water-filling solution.

$$P_k = max\left\{v - \frac{1}{\gamma_k}, 0\right\} \tag{14}$$

where $\gamma_k = |H_k|^2 / N_0 \Delta f$ and v is a constant (the "water-level") determined based on the total available power $P_{tx} = \sum_k P_k$. The resulting strategy of power allocation is illustrated in Fig. 11.

To illustrate the capacity, let us take one of the ocean channel frequency attenuation models, shown in dB in Fig. 9. The simple exponential model (10) is convenient due to its cubic range dependence, as pointed out in Section 4.3. Other relevant parameters are: $W = 6.25$ MHz, $K = 1024$. For the sake of building a conservative estimate of the channel capacity that we could rely on in more general conditions, we set the noise PSD value somewhat higher than the measurements in the ocean showed, namely to $N_0 = -155$ dBm/Hz.

Range variant capacity of the channel is calculated from (13) for $|H_k|^2$ given by a specific model. Fig. 12 shows that moving from 0.8 m to 1 m results in about 0.4 Mbps decrease in capacity, while 1–1.2 m change causes roughly 0.1 Mbps decline at $P_{tx} = 1$ W.

Fig. 13 shows the capacity as a function of distance for different power budgets. It indicates that the capacity of deep ocean RF channel is on the order of ten Mbps for distances within half a meter radius and 1 W of transmit power. This relatively large value motivates a vision of a guided ROV and very fast point-to-point data offload at short distance from a data collection port. As mentioned in the introduction, this technology supports the vision of a subsea positioning system that could be used to guide ROVs to data collection sites where data is transferred at tens of Mbps.

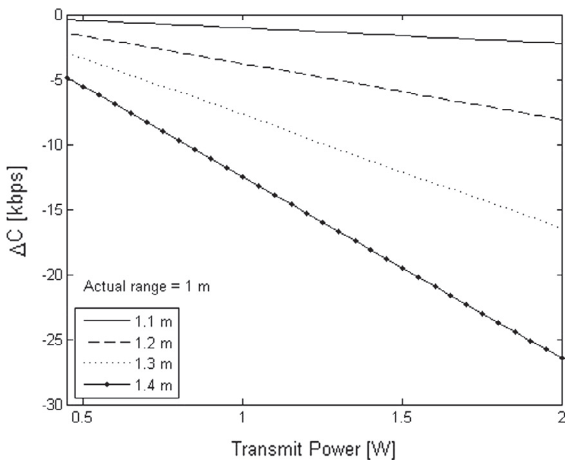

(a) [Underestimated range]

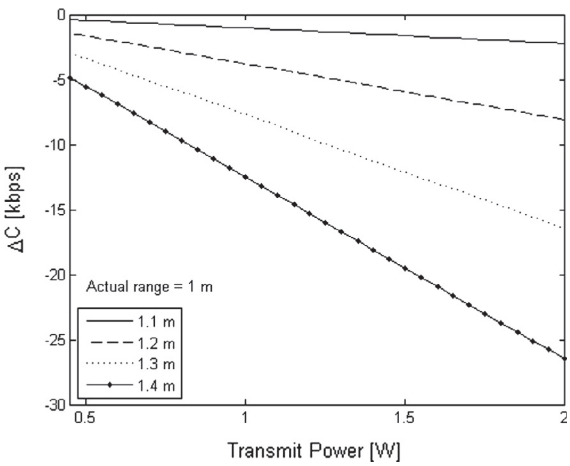

(b) [Overestimated range]

Fig. 14. Difference between the achievable bit rate and the channel capacity at the range of 1 m. Various curves correspond to different values of the estimated range.

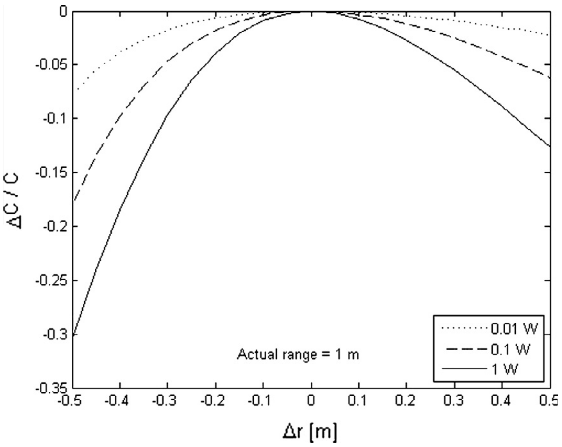

Fig. 15. Relative rate loss as a function of range estimation error.

5.1. The impact of range uncertainty on the achievable bit rate

The results of Figs. 12 and 13 indicate a rather large variation in capacity with range. Since the notion of capacity is based on the assumption that the range is perfectly known, the question naturally arises as to what bit rate is achievable when the range between the transmitter and receiver is not perfectly known, but can only be estimated with some finite accuracy.

To illustrate the impact of the range uncertainty on the achievable bit rate, let us assume that the transmitter uses an estimate $\hat{r}$ instead of the true range r to allocate the power. Power allocation is thus performed according to the expression (14) with $\gamma_k = |H(\hat{r}, f_k)|^2 / N_0 \Delta f$. Using the so-obtained values P_k, the achievable bit rate R_b is determined according to the expression (13) using the actual channel response $H_k = H(r, f_k)$. Fig. 14 shows the difference $\Delta C = R_b - C$ as a function of the total power for several values of the estimated range $\hat{r}$ corresponding to the actual range r = 1 m. We note that the loss increases with power; however, so does the capacity. At 1 W of transmit power and 1 m range, the rate loss is within 10 kbps for the range estimation error within 30%. This loss is relatively small compared to the capacity of 150 kbps. At 1 W of power and the true range of 1 m the achievable bit rate suffers a reduction of 30 kbps with estimated range of 0.6 m, or 15 kbps with 1.4 m.

Fig. 15 shows the relative rate loss, $\Delta C / C$, as a function of the range error $\Delta r = \hat{r} - r$. We note that underestimating the range leads to a higher loss than overestimating. That can be explained by the fact that the optimization algorithm allocates power to upper, more lossy channels. With the actual range of 1 m and transmit power of 1 W, relative loss is 20% for $\hat{r}$ = 0.6 m (Δr = −0.4 m) and 10% for $\hat{r}$ = 1.4 m (Δr = 0.4 m).

6. Conclusion

We measured electromagnetic field radiated by a pair of electrodes in a plastic tank in our lab and in the ocean, and modeled the magnitude and phase of the channel transfer function based on the measurements. Dipole radiation theory in conducting medium was helpful in predicting the general form of the channel transfer function.

A rational-polynomial model provided the best match for the recorded magnitude characteristic, especially at low frequencies, where simple exponential models failed to capture the near-field effect. Beyond a peak frequency, exponential model with linear frequency dependence of the attenuation constant gave a better match than the one with square root of frequency in the exponent, but was still outperformed by the rational-polynomial model. The simple exponential models were helpful in detecting near-field magnitude behavior.

Based on the simple exponential channel frequency response model, we established the channel capacity as a function of the transmit power and range, showing that this channel can support transmission at rates on the order of hundred Mbps over 10 cm range and ten Mbps for distances within half a meter radius and 1 W of transmit power. Taking into account the possibility of range estimation error, we showed that at 1 W of power the achievable bit rate suffers a reduction of several tens of kbps. To counteract this loss, use of dependable range estimation techniques based on feedback is encouraged.

The large magnitude variation (20–25 dB) with frequency, and time-invariance of the channel motivate the design of an OFDM system with unequal bit loading, which is the subject of our future work. In addition, channel coding solutions that perform well in low SNR conditions, such as LDPC codes, are expected to be useful in extending the range of operation.

Acknowledgments

This research was made possible by the Student Program at GE Global Research, Grant No. G0003357, through Research Partnership to Secure Energy for America (RPSEA) project 08121-2902-03. Assistance was also provided by NSF CNS-1212999 and ONR: N00014-09-1-0700. We would like to thank Linear Technology corporation for providing an additional A/D converter demo circuit board that we used for noise distribution measurement in our work described here.

References

[1] A. Zoksimovski, M. Stojanovic, D. Sexton, and C. Rappaport. Underwater electromagnetic communications using conduction–channel characterization. In 7th ACM International Conference on Underwater Networks & Systems, November 5-6 2012.

[2] H. Momma, T. Tsuchiya, Underwater communication by electric current, in: OCEANS'76, IEEE, 1976, pp. 631–636.

[3] J. Joe, S.H. Toh, Digital underwater communication using electric current method, in: OCEANS 2007-Europe, IEEE, 2007, pp. 1–4.

[4] Zhiqiang Wu, Jiadong Xu, Bin Li, A high-speed digital underwater communication solution using electric current method, in: 2010 2nd International Conference on Future Computer and Communication (ICFCC), vol. 2, May 2010, pp. V2–14–V2–16.

[5] Brian Kelley, Kranthi Manoj, Mo Jamshidi, Broadband rf communications in underwater environments using multi-carrier modulation, in: Systems, Man and Cybernetics, 2009, IEEE International Conference on SMC 2009, IEEE, 2009, pp. 2303–2308.

[6] A.I. Al-Shamma'a, A. Shaw, S. Saman, Propagation of electromagnetic waves at mhz frequencies through seawater, IEEE Trans. Antennas Propag. 52 (11) (2004) 2843–2849.

Please cite this article in press as: A. Zoksimovski et al., Underwater electromagnetic communications using conduction – Channel characterization, Ad Hoc Netw. (2015), http://dx.doi.org/10.1016/j.adhoc.2015.01.017

[7] X. Che, I. Wells, G. Dickers, P. Kear, X. Gong, Re-evaluation of rf electromagnetic communication in underwater sensor networks, IEEE Commun. Mag. 48 (12) (2010) 143–151.

[8] Kenneth P Hunt, James J Niemeier, Anton Kruger, Rf communications in underwater wireless sensor networks, in: 2010 IEEE International Conference on Electro/Information Technology (EIT), IEEE, 2010, pp. 1–6.

[9] C.A. Balanis, Antenna Theory, Analysis and Design, Hoboken, NJ, Wiley, NJ, 2005.

[10] T.M. Cover, J.A. Thomas, Elements of Information Theory, Wiley, 2006.

Arsen Zoksimovski graduated from the University of Novi Sad, Serbia, in 2000, and received the M.S. degree in electrical engineering from the University of New Hampshire in 2004. After receiving his M.S. degree, He worked as an R&D engineer in the area of digital signal processing and wireless communications. His interests as a researcher are centered on digital communication theory and electromagnetic wave propagation. He is currently pursuing Ph.D. degree in electrical engineering at Northeastern University, Boston MA.

Daniel Sexton is a Project Leader working for GE's Global research department in New York, he has been leading and participating in research projects in wireless communications and wireless sensor system development and Medical Systems MRI development. He has over 25 years of experience in industrial automation, controls and communications working for GE Fanuc and GE Industrial and has spent the last 14 years working at GE Global Research on various communications, controls and sensing technologies. His current research focus area is communications technologies in extremely harsh environments with demanding requirements working closely with various GE businesses and key technology providers to develop ecosystems which bring these technologies to market.

He holds over 35 granted US patents in both the communications and automation technologies. He is currently the co-chair for ISA100.11, a standards committee to define wireless systems for industry which released their first standard in 2009 and published the first revision in 2010, the core standard was approved by ANSI and subsequently by IEC (IEC 62734) in 2013. He is an active member of several IEEE 802 committees, and the IEEE 1588 committee defining the standards for the Industrial Internet and Deterministic Ethernet. Daniel is a past member of the advisory board for the Center for Automation Technologies and Systems at Rensselaer Polytechnic Institute. He holds a Bachelors (1978) and Masters degree (1982) in Electrical Engineering from Virginia Tech.

Milica Stojanovic graduated from the University of Belgrade, Serbia, in 1988, and received the M.S. ('91) and Ph.D. ('93) degrees in electrical engineering from Northeastern University, Boston, MA. She was a Principal Scientist at the Massachusetts Institute of Technology until 2008, when she joined Northeastern University where she is currently a Professor of electrical and computer engineering. She is also a Guest Investigator at the Woods Hole Oceanographic Institution, and a Visiting Scientist at MIT. Her research interests include digital communications theory, statistical signal processing and wireless networks, and their applications to underwater acoustic systems. She is an Associate Editor for the IEEE Journal of Oceanic Engineering, Associate Editor of the IEEE Transactions on Signal Processing, Chair of the IEEE Ocean Engineering Society's Technical Committee for Underwater Communications, Advisory Board member of the IEEE Communication Letters, and Editorial Board member of the Elsevier Physical Communication Journal. She is a Fellow of the IEEE.

Carey Rappaport (IEEE M, SM 96, F 06) received five degrees from the Massachusetts Institute of Technology: the SB in Mathematics, the SB, SM, and EE in Electrical Engineering in June 1982, and the Ph.D. in Electrical Engineering in June 1987. He is married to Ann W. Morgenthaler, and has two children, Sarah and Brian.

He has worked as a teaching and research assistant at MIT from 1981 until 1987, and during the summers at COMSAT Labs in Clarksburg, MD, and The Aerospace Corp. in El Segundo, CA. He joined the faculty at Northeastern University in Boston, MA in 1987. He has been Professor of Electrical and Computer Engineering since July 2000. During fall 1995, he was Visiting Professor of Electrical Engineering at the Electromagnetics Institute of the Technical University of Denmark, Lyngby, as part of the W. Fulbright International Scholar Program. During the second half of 2005, he was a visiting research scientist at the Commonwealth Scientific Industrial and Research Organisation (CSIRO) in Epping Australia. He has consulted for CACI, Alion Science and Technology, Inc., Geo-Centers, Inc., PPG, Inc., and several municipalities on wave propagation and modeling, and microwave heating and safety. He was Principal Investigator of an ARO-sponsored Multidisciplinary University Research Initiative on Humanitarian Demining, Co-Principal Investigator and Associate Director of the NSF-sponsored Engineering Research Center for Subsurface Sensing and Imaging Systems (CenSSIS), and Co-Principal Investigator and Deputy Director of the DHS-sponsored Awareness and Localization of Explosive Related Threats (ALERT) Center of Excellence.

He has authored over 400 technical journal and conference papers in the areas of microwave antenna design, electromagnetic wave propagation and scattering computation, and bioelectromagnetics, and has received two reflector antenna patents, two biomedical device patents and three subsurface sensing device patents. He was awarded the IEEE Antenna and Propagation Society's H.A. Wheeler Award for best applications paper, as a student in 1986. He is a member of Sigma Xi and Eta Kappa Nu professional honorary societies.